J. Fluid Mech. (1977), *vol.* 83, *part* 1, *pp.* 83–95
Printed in Great Britain

Stability of time-dependent double-diffusive convection in an inclined slot

By C. F. CHEN AND R. D. SANDFORD
Mechanical, Industrial and Aerospace Engineering Department,
Rutgers University, New Brunswick, New Jersey 08903

(Received 14 February 1977)

The two-dimensional motion of a stably stratified fluid containing two solutes with different molecular diffusivities in an inclined slot has recently been examined by Chen (1975, hereafter referred to as I). The two solutes have continuous opposing gradients with the slower-diffusing one more dense at the bottom. It is found that, in the steady state, there exists a slow upward flow along the slope driven by the slight buoyancy difference near the wall, not unlike the solution found by Wunsch (1970) and Phillips (1970) for a single solute. For the time-dependent flow resulting from switching on the diffusivities at $t = 0$, there may be a flow reversal near the wall depending on the relative magnitude of λ and τ (where λ is the ratio of the density gradient and τ^{-1} is the ratio of the diffusivity of the faster-diffusing solute T to that of the slower-diffusing one S). By examining the distributions of S and T across the slot, it becomes apparent that in cases with flow reversal double-diffusive instability is likely to occur.

In this paper, we examine the stability of time-dependent double-diffusive convection in an inclined slot both analytically and experimentally. The time-dependent perturbation equations are numerically integrated starting with an initial distribution of small random disturbances in the vorticity. The growth or decay of the kinetic energy of the perturbations serves to indicate whether the flow is unstable or stable. The results show that the flow becomes more unstable (*a*) with increasing λ at a given angle of inclination with respect to the vertical and (*b*) with increasing angle of inclination at a given value of λ. Experiments were carried out in a 2·54 cm wide slot using sugar and salt solutions at angles of inclination of 30°, 45° and 60°. Results obtained confirm the trends predicted by the analysis. Good agreement was obtained between the predicted and the experimental values of the critical wavelength for the case $\lambda = 0{\cdot}7$.

1. Introduction

It is known (Wunsch 1970; Phillips 1970) that when a stably stratified fluid containing one solute is placed in an inclined slot, the lines of constant density must be normal to the walls to satisfy the non-diffusive boundary condition there. This slight curving of the constant-density lines near the lower (upper) wall generates a buoyancy excess (deficit), thus causing an upward (downward) flow. The case in which the stably stratified fluid contains two solutes with different molecular diffusivities is examined by Chen in I. The two solutes have opposing gradients with the slower-diffusing one more dense at the bottom. It is found that under steady-state conditions the fluid

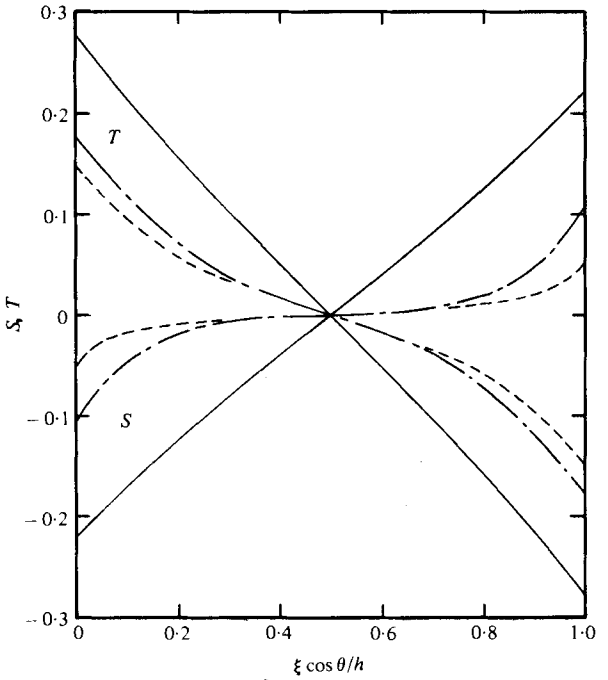

FIGURE 1. Distribution of S and T across the slot at $t = 0{\cdot}05$ for $\theta = 45°$ and $\tau = \frac{1}{3}$. ——, $\lambda = 0{\cdot}8$; —·—, diffusion; – – – –, $\lambda = 0{\cdot}2$.

behaves in the same manner as that containing only one solute. However, under time-dependent conditions resulting from switching on the diffusivities at $t = 0$, there may be a flow reversal near the wall depending on the relative magnitude of λ and τ, where

$$\lambda = \alpha \frac{\partial T}{\partial \zeta} \Big/ \beta \frac{\partial S}{\partial \zeta}, \tag{1}$$

in which T and S denote the faster- and slower-diffusing component, respectively, ζ denotes the vertical co-ordinate, $\alpha = -\rho^{-1}\partial\rho/\partial T$ and $\beta = \rho^{-1}\partial\rho/\partial S$, and $\tau = \kappa_S/\kappa_T$, where κ_S and κ_T are the molecular diffusivities of S and T. The density of the fluid is

$$\rho = \rho_0[1 - \alpha(T - T_0) + \beta(S - S_0)], \tag{2}$$

where the subscript zero denotes reference values at $\zeta = 0$. For $\lambda > \tau$, the flow along the lower wall is initially downward. The magnitude of the downward flow is a function of λ, being greater at larger values of λ. The reverse flow gradually decays and the flow eventually approaches the steady-state value. For $\lambda < \tau$, the approach to the steady state is monotonic.

If we examine the distributions of S and T across the slot, it will become clear that when reverse flow is present double-diffusive instability is likely to occur. In figure 1, distributions of S and T along $\zeta = 0$ at $t = 0{\cdot}05$ in a slot inclined at 45° are shown. These results were obtained by using the computer program developed in I. The horizontal co-ordinate ξ is rendered non-dimensional by $h/\cos\theta$, where h is the width of the slot and θ the angle of inclination from the vertical. The curves labelled 'diffusion' are the results for a hypothetical case in which the fluid is constrained not

to move; evolutions in S and T are due solely to diffusion. For $\lambda = 0{\cdot}2$, the flow is upward at the left wall and downward at the right wall. With this flow pattern, lighter T and heavier S are brought to the level $\zeta = 0$ near the left wall. As a result the concentration of T is less and that of S is greater than in the 'diffusion' case. For $\lambda = 0{\cdot}8$, a strong reverse flow occurs initially, bringing heavier T and lighter S to the $\zeta = 0$ level near the left wall. The resulting concentration of T is greater and that of S is less than in the 'diffusion' case. It is noted that in both the $\lambda = 0{\cdot}2$ and the $\lambda = 0{\cdot}8$ case the contributions to the density from T and S almost cancel out identically. The constant-density lines are practically horizontal.

For $\lambda = 0{\cdot}8$ any lateral movement of a parcel of fluid to the right along a constant-density line will bring the parcel into a region of smaller T and larger S concentration. Component T will equilibrate first, S lagging behind. As a result the parcel of fluid will experience a net buoyancy force. If this buoyancy force overcomes the viscous restraining force, vorticity will be generated. In the case $\lambda = 0{\cdot}2$, the net buoyancy force will be much smaller than that generated in the $\lambda = 0{\cdot}8$ case simply because the S contribution is so much smaller. It is then clear that, for a given value of θ, there will be a critical value of λ above which double-diffusive instability will occur. At larger values of λ, since the magnitude of the reverse flow is greater, the onset of instability will occur at an earlier time.

It is of interest to consider the case when the walls are vertical. The fluid will remain stationary since there are no unbalanced buoyancy forces near the two walls. The situation then is analogous to the heating of a solute gradient from below, which was considered first by Veronis (1965). For the case of opposing gradients of salt and sugar with large values of the Rayleigh numbers, the critical condition for onset of oscillatory instability is $\lambda \approx 1$. Since we are always dealing with statically stable cases ($\lambda < 1$), this type of instability would not be triggered in the present problem. The double-diffusive instability considered in this paper is induced by the peculiar S and T distributions brought about by the initial motion. In the following, we examine such instability phenomena both analytically and experimentally. The anticipated results are borne out by the analysis and confirmed by the experiments.

2. Stability analysis

Consider two-dimensional motion of a fluid containing two components T and S in an infinite slot of width h which is inclined at an angle θ with respect to the vertical axis ζ. The initial T gradient $\partial T/\partial\zeta$ is positive and the initial S gradient $\partial S/\partial\zeta$ is negative with the ratio of the density gradients $\lambda < 1$, so that the fluid is statically stable. Let the z axis be along the lower wall of the slot and the x axis be normal to that wall (see figure 2). Let the T and S distributions be

$$\left.\begin{aligned} T &= T_0 + z\cos\theta + T_1(x,t) + T'(x,z,t), \\ S &= S_0 - z\cos\theta + S_1(x,t) + S'(x,z,t), \end{aligned}\right\} \tag{3}$$

where the subscripts zero denote reference values at $\zeta = 0$, the subscripts one denote values in the basic state and the primes denote perturbations. Let the vorticity be

$$\omega = \omega_1(x,t) + \omega'(x,z,t). \tag{4}$$

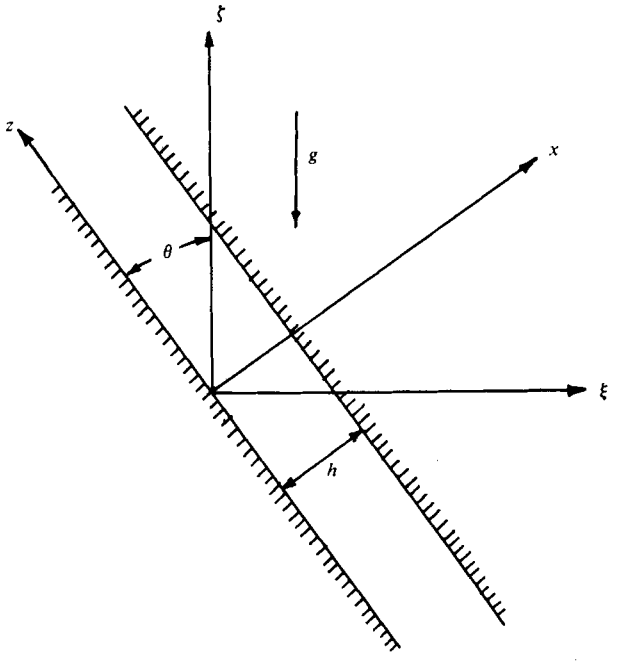

FIGURE 2. Co-ordinate system.

Equations governing T_1, S_1 and ω_1 and solutions thereof are given in I. Neglecting second-order terms, the perturbation equations are

$$\frac{1}{\sigma}\left[\frac{\partial\omega'}{\partial t}+u'\frac{\partial\omega_1}{\partial x}+w_1\frac{\partial\omega'}{\partial z}\right]=\nabla_2^2\omega'+R_S\cos\theta\left[\lambda\frac{\partial T'}{\partial x}+\frac{\partial S'}{\partial x}\right]-R_S\sin\theta\left[\lambda\frac{\partial T'}{\partial z}+\frac{\partial S'}{\partial z}\right], \quad (5)$$

$$\frac{\partial T'}{\partial t}+u'\frac{\partial T_1}{\partial x}+w_1\frac{\partial T'}{\partial z}+w'\cos\theta=\nabla_2^2T', \quad (6)$$

$$\frac{\partial S'}{\partial t}+u'\frac{\partial S_1}{\partial x}+w_1\frac{\partial S'}{\partial z}-w'\cos\theta=\tau\nabla_2^2S', \quad (7)$$

$$\omega'=\nabla_2^2\psi',$$

$$\nabla_2^2=\frac{\partial^2}{\partial x^2}+\frac{\partial^2}{\partial z^2}, \quad (u',w')=\left(\frac{\partial}{\partial z},-\frac{\partial}{\partial x}\right)\psi', \quad (8)$$

with boundary conditions

$$u'=w'=\partial T'/\partial x=\partial S'/\partial x=0 \quad \text{at} \quad x=0,1. \quad (9)$$

The S-Rayleigh number is defined as $R_S=-g\beta(\partial S/\partial\zeta)_0h^4(\nu\kappa_T)^{-1}$, in which g is the gravitational acceleration and ν is the kinematic viscosity; $\sigma=\nu/\kappa_T$. All quantities in the above set of equations are non-dimensional, with h as the characteristic length, h^2/κ_T as the characteristic time and $h\partial T/\partial\zeta$ and $-h\partial S/\partial\zeta$ as characteristic values of T and S, respectively. Previous experiments showed that the instabilities manifest

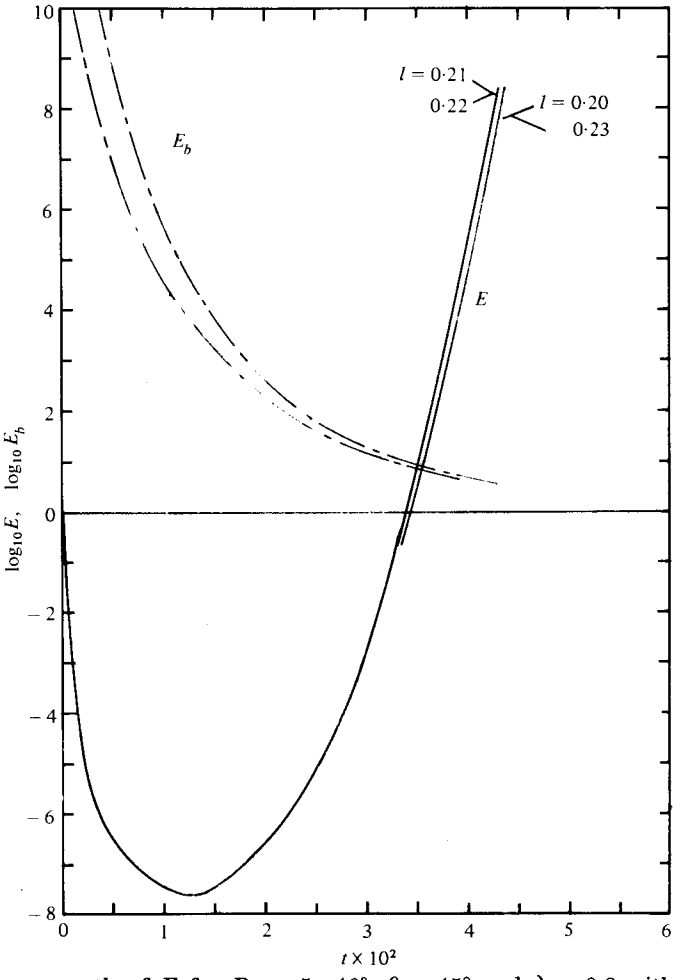

FIGURE 3. ——, growth of E for $R_S = 5 \times 10^8$, $\theta = 45°$ and $\lambda = 0{\cdot}8$ with different assumed values of l. The critical wavelength l_c is 0·21. —·—·—, upper and lower limits of kinetic energy of the basic flow E_b with a period of oscillation of $3{\cdot}335 \times 10^{-4}$.

themselves as horizontal cellular flow patterns along the wall. We therefore assume that all variables are periodic in z with wavelength l, e.g.

$$\omega'(x, z, t) = \tilde{\omega}'(x, t) \exp(2i\pi z/l), \tag{10}$$

where $\tilde{\omega}'$ is complex. Upon substituting these quantities into the perturbation equations (5)–(8) and separating the real and imaginary parts, we obtain eight simultaneous equations describing the time evolution of ω', T', S' and ψ'.

This set of equations, together with the equations governing the time-dependent basic flow, is numerically integrated forwards in time starting with a distribution of small random perturbations in ω'. This method has been used by Chen (1974) to investigate the stability of the convective flow induced in a stably stratified fluid under lateral heating. It was shown there that consistent results could be obtained whether the random disturbances were in S', T' or ω'.

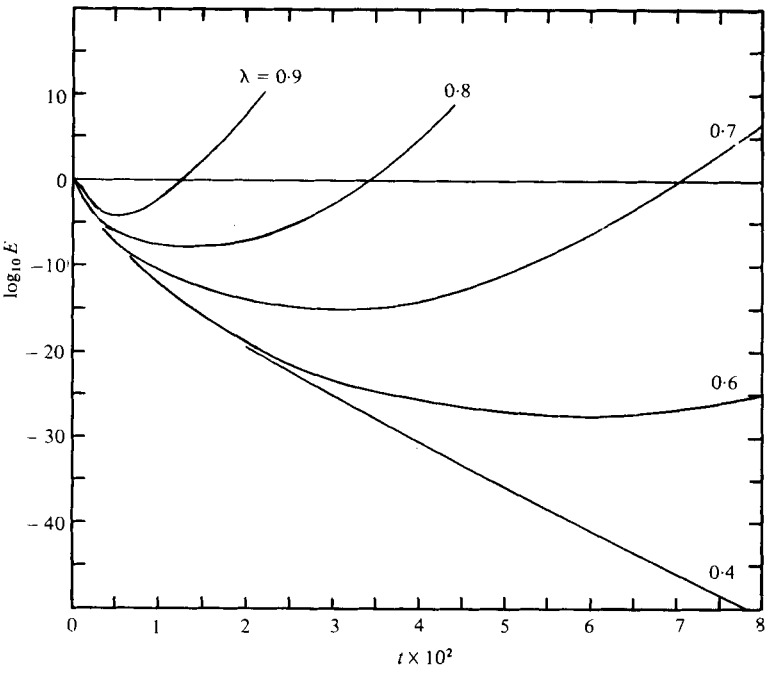

FIGURE 4. Effect of λ on growth of E for $R_S = 5 \times 10^8$, $\theta = 45°$ and $l = 0{\cdot}2$.

Random perturbations in vorticity were generated by using the subroutine RANDU of the IBM Scientific Subroutine Package. The magnitude of the perturbations was limited to be less than $0{\cdot}5 \times 10^{-4}$. With this assumption, the initial kinetic energy of the perturbation flow was of the order of 10^{-12}. An explicit scheme was used for time integration. In order to ensure numerical stability $\Delta t < 0{\cdot}5\Delta x^2/\sigma$. If the solutes were sugar and salt σ was approximately 700, in which case the time step became extremely small. It was shown in I that the time-dependent velocity profiles calculated with $\sigma = 7$ and 700 were substantially the same. Since the onset of instabilities was related to the distributions of S and T, which in turn depended on the history of the velocity profile, we carried out the stability calculations with $\sigma = 7$. On the basis of the experience of I, Δx was set to be 0·02. The equations relating ω' to ψ' were solved by inverting a tridiagonal matrix using the method of Gaussian elimination. The stability of the numerical scheme was checked by two methods. One was to start the calculations with no perturbations. In this case, all perturbation quantities remained zero; the motion was the same as that generated in I. The other was to start the calculations with $\lambda = 0$, for which the flow was known to be stable. The perturbation kinetic energy decayed steadily. All calculations reported in the paper were made with $\tau = \frac{1}{3}$.

Results are presented in terms of the time evolution of the kinetic energy of the perturbation E normalized by its initial value. A typical growth curve is shown in figure 3 for $\theta = 45°$ and $R_S = 5 \times 10^8$. The disturbances decay initially because S and T distributions due to diffusion alone are basically stable. After $t \cong 0{\cdot}013$, E grows super-exponentially. To determine the critical wavelength, calculations were made with systematic variations in l. That wavelength which gives the fastest growth of E is the critical one. For the present case $l_{cr} = 0{\cdot}21$, although on the scale of the graph the difference between the E-curves for $l = 0{\cdot}20$ and 0·21 is not discernible.

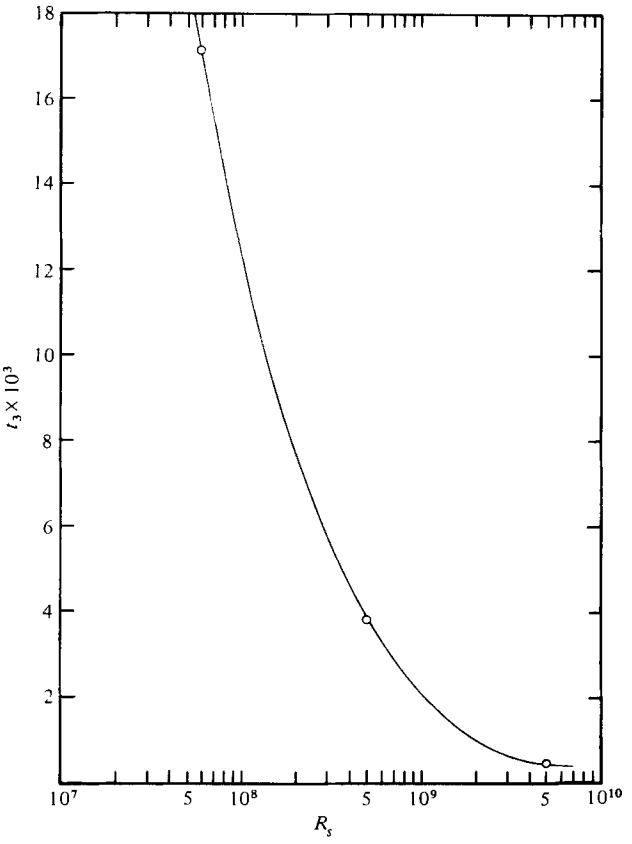

FIGURE 5. Effect of Rayleigh number on the time when the kinetic energy of the perturbations has grown to a thousand times its initial value.

	$\lambda = 0{\cdot}9$		
θ	30°	45°	60°
$t_0 \times 10^2$	2·123	1·267	1·104
$t_3 \times 10^2$	2·415	1·548	1·410
γ	23·68	24·62	22·57
l_{cr}	0·20	0·22	0·31
	$\lambda = 0{\cdot}8$		
$t_0 \times 10^2$	5·685	3·384	2·716
$t_3 \times 10^2$	6·080	3·745	3·170
γ	17·50	19·14	15·19
l_{cr}	0·18	0·21	0·33
	$\lambda = 0{\cdot}7$		
$t_0 \times 10^2$	12·11	6·846	5·638
$t_3 \times 10^2$	12·71	7·295	6·164
γ	11·40	15·39	13·13
l_{cr}	0·18	0·22	0·32

TABLE 1. Effect of angle of inclination.

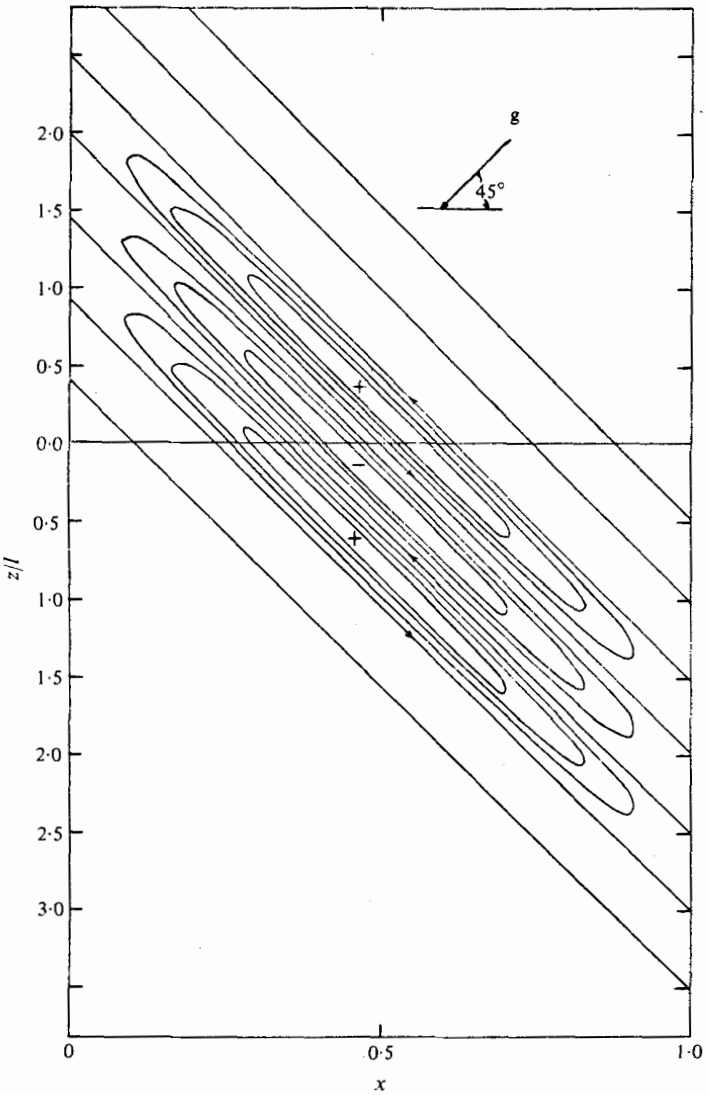

FIGURE 6. Perturbation streamlines at $t = 4{\cdot}2 \times 10^{-2}$ for $R_S = 5 \times 10^8$, $\theta = 45°$ and $l_{cr} = 0{\cdot}21$. $\psi = 0, \pm 3, \pm 5, \pm 7 \times 10^{-5}$.

The growth rate γ (if $E = E_0 \exp \gamma t$), however, is $1{\cdot}883 \times 10^3$ for $l = 0{\cdot}20$ and $1{\cdot}194 \times 10^3$ for $l = 0{\cdot}21$. When E reaches 10^8, the perturbation kinetic energy is of the order of 10^{-5} while that of the basic flow is of order unity. The kinetic energy of the basic flow is also shown in figure 1. It increases almost impulsively to a value of the order of 10 then decreases to the steady-state value with a damped oscillation of period $3{\cdot}335 \times 10^{-4}$, which is somewhat larger than the period $2{\cdot}375 \times 10^{-4}$ of natural oscillations based on the overall density gradient. For a slot width of 2·54 cm and $\kappa_T = 1{\cdot}6 \times 10^{-5}$ cm^2/s, $t = 10^{-4}$ corresponds to 40 s. Since the period of the oscillations is too small to be clearly shown in the figure, we have presented only the upper and lower limits of the oscillations.

It was conjectured in I that, since the magnitude of the reverse flow decreases with decreasing λ at a given angle of inclination, stability is enhanced as λ is decreased.

This conjecture is confirmed by the results shown in figure 4, in which the growth of E is shown for λ decreasing from 0·9 to 0·4 for $\theta = 45°$ and $R_S = 5 \times 10^8$. As λ is decreased, the initial damping becomes stronger, reflecting the fact that the initial S and T profiles, due to diffusion, persist for longer periods of time, and the subsequent rates of growth become smaller. For $\lambda = 0{\cdot}4$, E exhibits exponential decay, indicating that the flow is stable. The time when the growth curve crosses the $E = 1$ line may serve as a rough measure of the onset time of instabilities.

When R_S is reduced at constant values of λ and θ, the onset of instabilities occurs at later times. This effect is shown in figure 5, in which the time t_3 for E to reach 10^3 is shown as a function of R_S for $\lambda = 0{\cdot}8$ and $\theta = 45°$. For $R_S \leqslant 5 \times 10^6$, the flow is stable.

The effect of the angle of inclination on the relative times of onset of instabilities is summarized in table 1. The times t_0 and t_3 (when E reaches 10^0 and 10^3, respectively), the average growth rate γ between these two times and the critical wavelengths are tabulated for $\theta = 30°$, 45° and 60° and $\lambda = 0{\cdot}9$, 0·8 and 0·7. For a given value of λ, the onset of instabilities will occur earlier when θ is increased. The growth rate of E, however, shows a maximum at $\theta = 45°$. The critical wavelength exhibits an increasing trend with θ, with a large jump from $\theta = 45°$ to 60°.

The perturbation streamlines are shown in figure 6 for $R_S = 5 \times 10^8$ and $\theta = 45°$ at $t = 4{\cdot}2 \times 10^{-2}$ when $E = 10^4$. The flow pattern exhibits counter-rotating vortices of equal size. Experimental observations show that layers with negative vortices are of very small thickness while those with positive vortices usually take up the entire l_{cr}. In fact the negative vortices appear as a shear layer across which u changes sign. Since the perturbed flows near walls in positive vortices are in the same direction as the basic flow and vice versa for negative vortices, the positive vortices will probably grow at the expense of the negative ones. This conjecture requires further analysis.

3. Experiment

Experiments were carried out in a Plexiglas container $2{\cdot}54 \times 7{\cdot}62 \times 66$ cm long. The base of this long narrow tank was set at 45° with respect to the walls. With an appropriate support system, this tank may be inclined at either 30° or 60° from the vertical. The tank was filled with sugar–salt solution having continuous opposing gradients with sugar more dense at the bottom by the two-container method of Oster (1965) with a filtering float to minimize mixing as described by Turner & Chen (1974). A small flow rate was used during filling, and it generally took 13 min to fill the tank.

For a given θ, the density of the sugar solution was maintained constant; the density of the salt solution was varied according to the required value of λ. It is known that the viscosities of pure sugar solution and pure salt solution increase with solute content. The viscosity of sugar–salt solution, however, cannot be found in general reference books. With the help of Mr R. A. Paliwal, we measured the kinematic viscosity of sugar–salt solutions using Cannon–Fenske viscometers. The data are shown in figure 7; the equation for the least-squares curve is

$$\nu/\nu_0 - 1 = 0{\cdot}01281C - 0{\cdot}00023C^2 + 0{\cdot}00003C^3,$$

where ν_0 is the viscosity of the pure sugar solution and C the percentage concentration of salt.

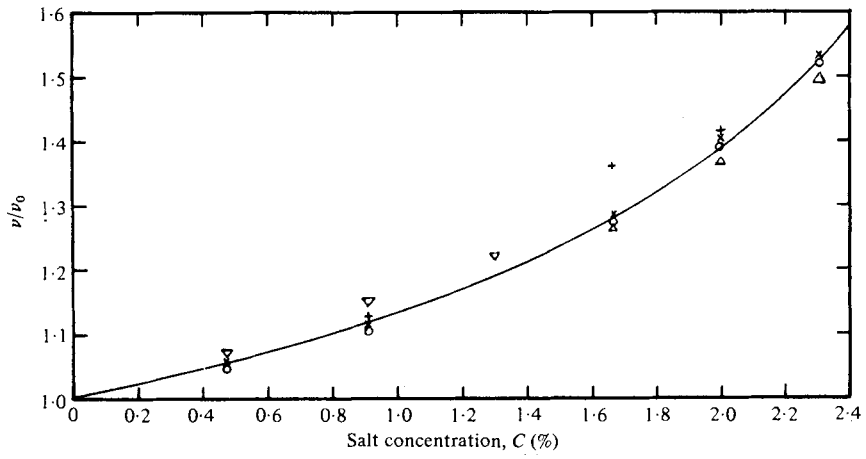

FIGURE 7. Viscosity data for sugar–salt solutions at $30{\cdot}0 \pm 0{\cdot}1$ °C. ν_0 is the kinematic viscosity of a solution containing no salt. Sugar content: ○, 0; △, 4·76 %; ×, 9·09 %; +, 16·67 %; ▽, 23·08 %.

Since the Rayleigh number R_S depended on the sugar gradient $\partial S/\partial\zeta$ and the product $\kappa_T \nu$, whose variation along the tank depended on the concentrations of salt and sugar, an iterative method was used to determine the value of $\partial S/\partial\zeta$ which would give $R_S \cong 5 \times 10^8$ at the mid-height of the tank. A total of twelve tests were made, four at $\theta = 60°$, five at $\theta = 45°$ and three at $\theta = 30°$. At $\theta = 30°$ and $\lambda = 0{\cdot}8$ a saturated salt concentration was encountered and it was necessary to reduce the fluid-column length by about 10 % to give the desired R_S. This reduced column length was used for all tests with $\theta = 30°$. A summary of the test conditions is presented in table 2. There was a general stratification of R_S along the fluid column, especially at $\theta = 45°$ and 60°, because of the high concentration of sugar used. As a result, instabilities were observed to occur first near the top of the tank and to progress downward. The occurrence of instabilities in the form of horizontal layers was made visible by use of the shadowgraph technique. A 500 W uncollimated light source was placed approximately 3 m away from the tank. Shadows were observed on a piece of tracing paper fixed to the other side of the tank.

In all tests, the value of λ was limited to 0·8 or less. For $\lambda > 0{\cdot}8$, an entirely different basic flow was observed as described in Turner & Chen (1974): "Just above the sloping boundary a downflow formed, and above it an upslope counterflow, which did not continue indefinitely, but turned outwards to form a series of approximately equally spaced layers which developed fairly uniformly all along the plate. These advanced with well-defined fronts away from the slope,... behind each advancing front was a local reversal of relative vertical gradients to produce 'fingers' even though the original smooth distributions were in the opposite 'diffusive' sense." Our present analysis is not capable of treating such a complicated basic flow pattern. It is ironic that the present analysis, whose inception was inspired by the experimental observations described above, cannot yield a rational explanation of this phenomenon.

The sequence of events leading from onset to the gradual spreading of instabilities throughout the tank is best illustrated by series of photographs taken approximately 2 h apart for the case $\theta = 45°$ and $\lambda = 0{\cdot}6$ and shown in figure 8 (plate 1). The time

Test		1	2	3	4	5	6	7	8	12	9	10	11
θ			60°					45°				30°	
Maximum percentage of sugar			25·9					43·8				49·3	
λ		0·8	0·7	0·6	0·5	0·8	0·7	0·6	0·556	0·4	0·8	0·7	0·6
$\nu \times 10^2$ (cm^2/s)	top	1·21	1·15	1·13	1·12	1·353	1·28	1·21	1·18	1·12	1·44	1·31	1·21
	mid-section	1·45	1·44	1·43	1·42	2·10	2·05	2·02	2·00	1·95	2·28	2·24	2·18
	bottom		2·34					6·27				10·42	
$\kappa_T \times 10^5$ (cm^2/s)	top	1·64	1·62	1·61	1·59	1·84	1·79	1·74	1·72	1·66	1·96	1·873	1·81
	mid-section	1·57	1·56	1·55	1·54	1·65	1·63	1·61	1·60	1·55	1·69	1·66	1·64
	bottom		1·60					1·60				1·60	
$R_S \times 10^{-8}$	top	5·51	5·65	5·82	5·98	6·53	7·10	7·70	7·95	8·79	6·35	7·30	8·19
	mid-section	4·65	4·73	4·80	4·85	4·69	4·85	4·98	5·07	5·39	4·64	4·82	5·00
	bottom		2·83					1·62				1·072	

TABLE 2. Summary of test conditions. Values of ν and κ_T values are for 25 °C. κ_T is assumed to be independent of sugar content.

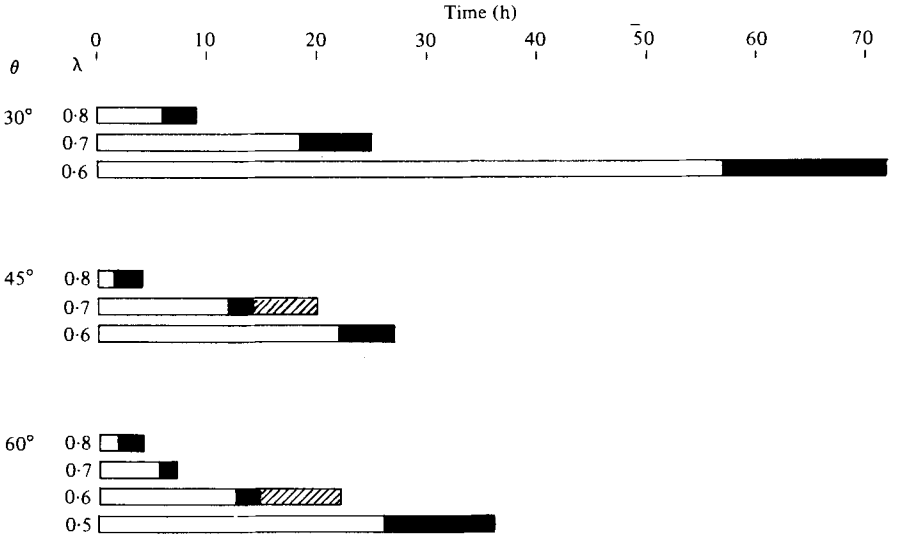

FIGURE 11. Observed onset time of cellular convection in the slot. The beginning of the dark bar denotes the time when half of the test tank is covered with layers. The end of the dark bar denotes the time when the entire tank is covered with layers. In the cross-hatched area no observations were made.

when each photograph was taken is denoted by a four-digit number (hours and minutes). Zero time corresponds to the start of the filling process. The instabilities were first observed at 16 h. By 29 h, horizontal layers appeared throughout the entire tank. This cellular pattern would persist for days, fading slowly owing to diffusion across the cell boundaries. The distance between the dark bands is a complete wavelength of the secondary flow. The motion in each cell is clockwise when viewed on the photograph, which corresponds to a positive vortex.

As λ is increased, the same sequence of events shifts forwards in time as illustrated by the photographs for $\lambda = 0{\cdot}7$ and $0{\cdot}8$ in figure 9 (plate 1). For $\lambda = 0{\cdot}7$, certainly by 21 h the layers were occurring throughout the tank. It was unfortunate that no observations were made between 12 and 21 h, since it was almost certain that the layers extended over the entire tank at some time before 21 h. For $\lambda = 0{\cdot}8$, the entire sequence of events took place within 4 h. It was at this highest value of λ tested that layers in formative stages became clearly visible on the shadowgraph. The advance of the instabilities from the top to the bottom was very rapid, which gave the appearance of simultaneous onset of instabilities over some portions of the tank. We include a photograph taken at 24 h, which shows that the layers were considerably thicker than those observed at 6 h. This gradual reduction of the number of layers by the process of erosion was found at all three angles at $\lambda = 0{\cdot}8$. At lower values of λ, the number of layers, or the thickness of each individual layer, stayed approximately constant until the time when the layers disappeared owing to salt and sugar diffusion.

The effect of the angle of inclination at $\lambda = 0{\cdot}6$ is shown in figure 10 (plate 2). Two photographs are shown for each θ, one for the initial stage and the other for the final stage of growth of instabilities. The steady shift towards earlier onset times as the angle of inclination is increased is clearly exhibited.

λ \ θ	30°	45°	60°
0·8	0·285	0·216	0·571
0·7	0·200	0·222	0·364
0·6	0·222	0·222	0·364

TABLE 3. Observed cell widths.

We summarize the observations about the effects of λ and θ in a more quantitative manner in figure 11. The beginning of the dark portion of the bar graph denotes the time when half the tank is covered with layers. The end of the dark bar denotes the time when the layers have grown to cover the entire tank. The cross-hatched portions signify that the end point lies somewhere in that region; the precise time was not observed. Except for the case $\lambda = 0{\cdot}8$ and $\theta = 45°$, the general trends predicted by theoretical considerations were confirmed. The average width of the cells measured along the wall non-dimensionalized with respect to the slot width is presented in table 3. For the case $\lambda = 0{\cdot}7$, these values are within 10% of the predicted critical wavelength listed in table 2. The agreement between the predicted and the observed values for $\lambda = 0{\cdot}8$ is not so good. This may be attributed to the uncertainty in the observed values owing to the cell erosion process mentioned above.

A test was carried out for $\lambda = 0{\cdot}4$ and $\theta = 45°$. On the sixth day, three layers had developed near the top. By the eighth day there were seven layers, which started to fade thereafter. By the ninth day there were only five left. In the rest of the tank, there were no layers at all. This observation agrees with the calculated result that the flow is stable as shown in figure 4.

The results of the analysis portion were presented at the 14th International Congress of Theoretical and Applied Mechanics, Delft, The Netherlands, in August 1976. The financial support of the National Science Foundation through Grant ENG 73-03545-A01 is gratefully acknowledged.

REFERENCES

CHEN, C. F. 1974 Onset of cellular convection in a salinity gradient due to a lateral temperature gradient. *J. Fluid Mech.* **63**, 563–576.

CHEN, C. F. 1975 Double-diffusive convection in an inclined slot. *J. Fluid Mech.* **72**, 721–729.

OSTER, G. 1965 Density gradients. *Scient. Am.* **213**, 70–76.

PHILLIPS, O. M. 1970 On flows induced by diffusion in a stably stratified fluid. *Deep-Sea Res.* **17**, 435–443.

TURNER, J. S. & CHEN, C. F. 1974 Two-dimensional effects in double-diffusive convection. *J. Fluid Mech.* **63**, 577–592.

VERONIS, G. 1965 On finite amplitude instability in thermohaline convection. *J. Mar. Res.* **23**, 1–17.

WUNSCH, C. 1970 On oceanic boundary mixing. *Deep-Sea Res.* **17**, 293–301.

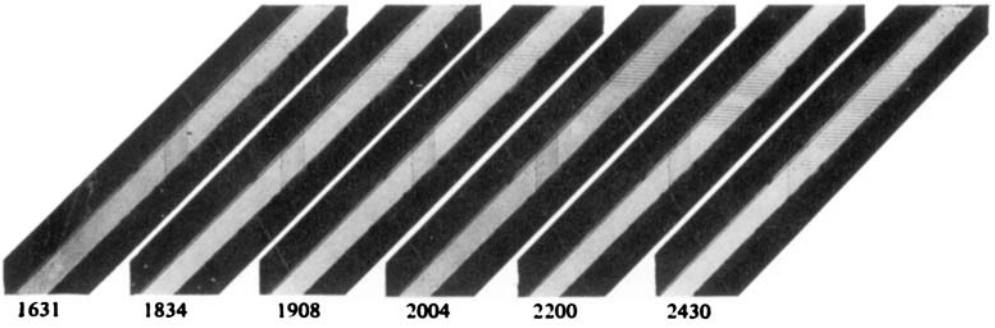

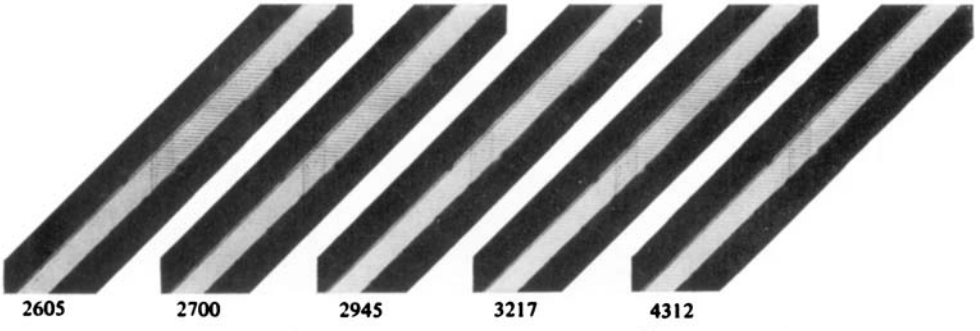

FIGURE 8. Development of layer convection for $\theta = 45°$ and $\lambda = 0{\cdot}6$.

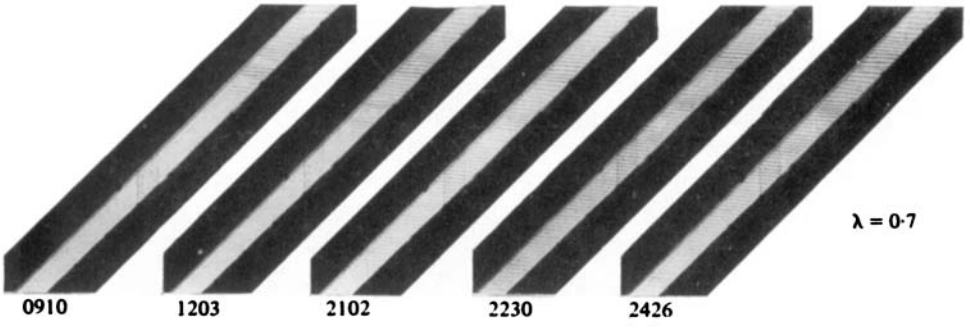

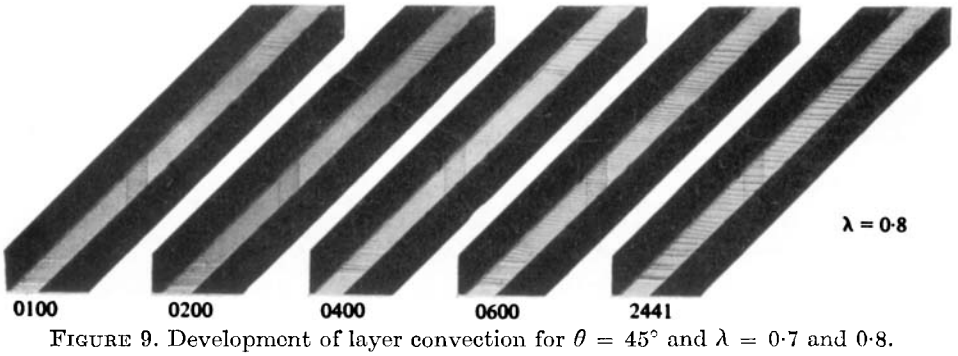

FIGURE 9. Development of layer convection for $\theta = 45°$ and $\lambda = 0{\cdot}7$ and $0{\cdot}8$.

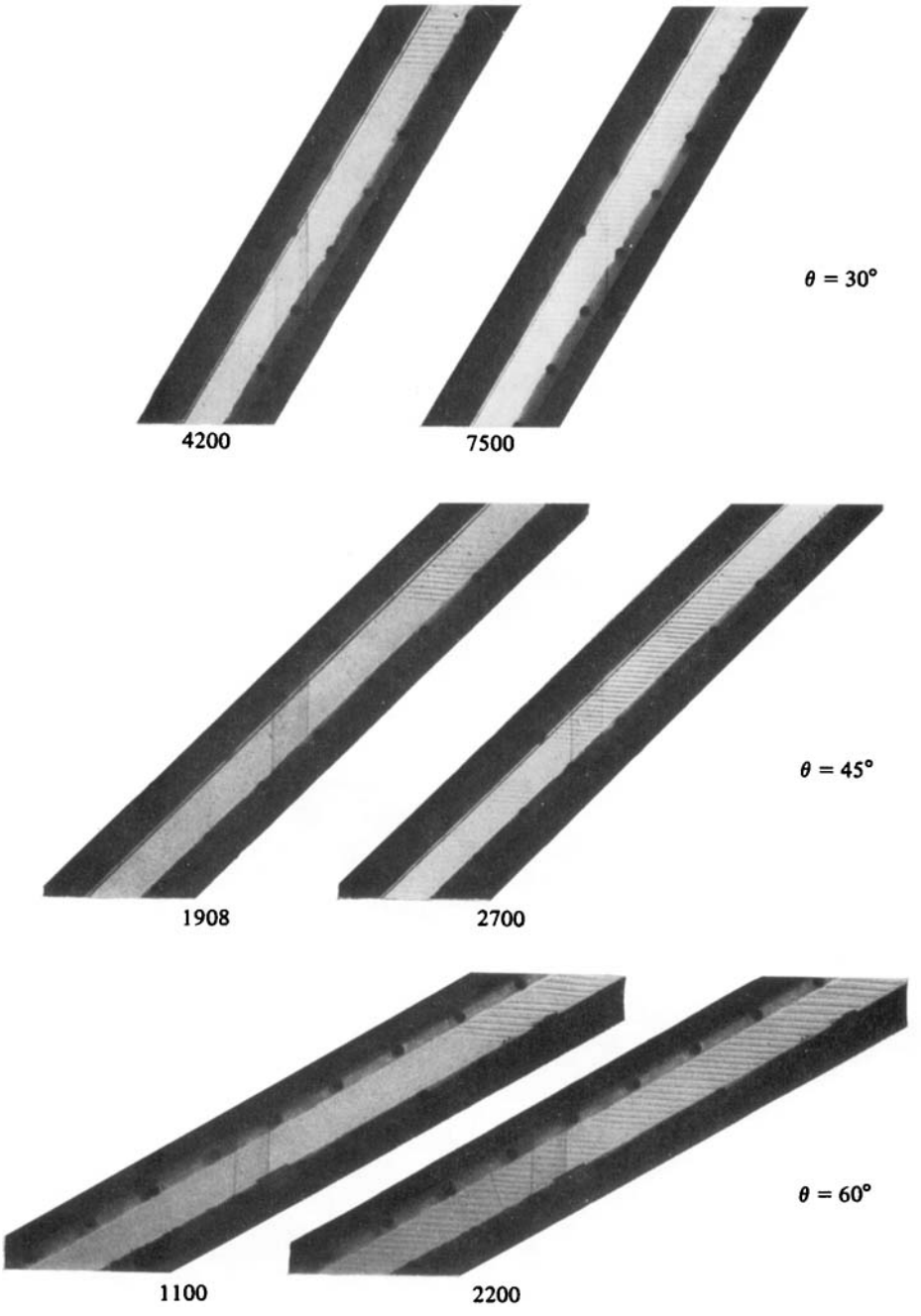

FIGURE 10. Effect of θ on layer development at $\lambda = 0{\cdot}6$.